Confined-acoustic-phonon-assisted cyclotron resonance in free-standing semiconductor quantum well structures

J. S. Bhat,* R. A. Nesargi, and B. G. Mulimani
Department of Physics, Karnatak University, Dharwad-580 003, India
(Received 20 July 2005; revised manuscript received 28 February 2006; published 29 June 2006)

Phonon-assisted cyclotron resonance (PACR) in a free-standing quantum well (FSQW) structure is studied when electrons are scattered by confined-acoustic modes through deformation potential. Elastic continuum model is employed to describe the confined-acoustic modes, that are classified as shear, dilatational, and flexural waves. Expression for the absorption coefficient is obtained. Numerical results are presented for the frequency, magnetic field, temperature, and well-width dependence of absorption coefficient in GaAs and GaN free-standing quantum well structures. In the extreme quantum limit only dilatational modes contribute for phonon-assisted cyclotron resonance. Results are compared with those based on bulk description of acoustic phonons and significant differences are noted. The calculations demonstrate that phonon-assisted cyclotron resonance studies can lead to a better understanding of confined electron-acoustic phonon interaction in free-standing quantum wells.

DOI: 10.1103/PhysRevB.73.235351 PACS number(s): 73.63.Hs, 78.20.Ls

I. INTRODUCTION

The interest in the study of electron-phonon interaction in semiconductor nanostructures, both in the presence of zero and finite quantizing magnetic fields, continues unabated.[1,2] An important effect relevant to any discussion of electron-phonon interaction in the presence of a magnetic field is the phonon-assisted cyclotron resonance (PACR), in which electron transition between the Landau levels due to absorption of a photon is accompanied by absorption or emission of a phonon. There exist in literature theoretical[3–6] and experimental[7,8] investigations of PACR in bulk semiconductors. PACR in two-dimensional quantum well structures[9–11] has been studied based on the bulk description of phonon modes. It is well established[12–17] that in widely studied quantum well structures, such as GaAs/AlAs, the acoustic and optical phonon modes are confined to respective layers. In addition, there exist interface modes localized in the vicinity of heterointerfaces. PACR in these QW structures have been studied[18,19] for confined optical phonon modes and interface modes. Additional peaks have been predicted in the absorption spectrum due to interface modes. However, the study of PACR when electrons are scattered by confined acoustic modes, though important, has not received attention.

Free-standing layers with a few-nanometer thickness are referred to as free-standing quantum well (FSQW) structures. Electron beam evaporation,[20] molecular beam epitaxy,[21] and standard lithographic techniques[22] have made possible the fabrication of FSQWs. These structures have features substantially different from conventional quantum heterostructures. In a free-standing and unstrained quantum slab, phonon dispersion changes due to spatial confinement induced by the free surface boundaries. The electron-confined-acoustic-phonon interaction manifests in its transport and optical properties. Experimental investigations of lattice thermal conductivity[23] in Si FSQWs have demonstrated the spatial confinement of acoustic phonons. To understand quantitatively electron transport and optical properties of these quantum structures, it is necessary to take into account the confinement of acoustic-phonon modes. The distinct features of phonon modes and their participation in optical absorption can easily be studied and identified in PACR studies.

With the application of a magnetic field perpendicular to the plane of a FSQW, the in-plane motion of the electron is quantized into Landau levels. This completely discrete energy spectrum leads to many interesting features in the electron transport and optical properties of the quantum slab. In this paper, following Bass and Levinson,[3] and the approach followed in our earlier work on QW structures, we present a theory of PACR in FSQWs employing perturbation technique. The confined-acoustic phonons are described by the elastic continuum model.[2,24,25] Calculations are presented for GaN with zinc-blende structure and GaAs structures. In Sec. II we outline the theory and present the expressions for the PACR absorption coefficient obtained for both the confined and bulk descriptions of phonon modes in FSQW. Numerical results for energy dispersion of confined acoustic modes in the case of GaAs and GaN free-standing quantum wells have been obtained and used in the calculations of PACR absorption coefficients. In Sec. III numerical results are presented for the frequency, magnetic field, temperature, and well-width dependence of absorption coefficient in GaAs and GaN free-standing quantum well structures. Results are compared with those based on bulk description of acoustic phonons.

II. THEORY

A. Basic equations

The absorption coefficient can be related to the transition probabilities for absorption and emission of photons. It can be expressed as[26]

$$K = \frac{\sqrt{\varepsilon}}{N_\nu c} \sum_i (W_i^{ab} - W_i^{em}) f_i, \tag{1}$$

where ε is the dielectric constant of the medium, N_ν is the number of photons in the radiation field, and f_i is the electron

distribution function. The sum is over all possible initial states i of the system. The transition probability for absorption (emission) of photons with simultaneous phonon absorption or emission $W_i^{ab(em)}$ is given by the Fermi golden rule,

$$W_i^{ab(em)} = \frac{2\pi}{\hbar}\sum_f |\langle f|M|i\rangle|^2 \delta(E_f - E_i \mp \hbar\Omega \mp \hbar\omega_p), \quad (2)$$

where $\langle f|M|i\rangle$ is the transition matrix element for the electron-photon-phonon interaction, E_i and E_f are the initial and final state energies of the electron, and $\hbar\Omega$ and $\hbar\omega_p$ are the energies of the photon and acoustic phonon, respectively. The sum is over all possible final states f of the system. The transition matrix elements can be written as[3]

$$\langle f|M|i\rangle = \sum_j \left[\frac{\langle f|H_{rad}|j\rangle\langle j|H_{el-ph}|i\rangle}{E_i - E_j \pm \hbar\omega_p} + \frac{\langle f|H_{el-ph}|j\rangle\langle j|H_{rad}|i\rangle}{E_i - E_j \pm \hbar\Omega} \right], \quad (3)$$

where H_{rad} and H_{el-ph} are the interaction Hamiltonian with the radiation field and phonons, respectively. The sum is over all the intermediate states j of the system.

B. Electron wave function and eigenvalues

We consider a FSQW structure where electrons are free to move in the x-y plane and a uniform static magnetic field **B** is applied in the z direction. Adopting a single band spherical effective mass model for electrons, the electron eigenfunctions ψ_{Nmk_y} and energy eigenvalues E_{Nm} can be expressed as[19]

$$\psi_{Nmk_y} = L_y^{-1/2}\phi_N(x - x_0)\exp(ik_y y)\chi_m(z), \quad (4)$$

and

$$E_{Nm} = (N + 1/2)\hbar\omega_c + m^2 E_0, \quad (5)$$

respectively. In the above equations, the Landau-level index $N=0,1,2,\ldots$, the electric subband quantum number $m=1,2,3,\ldots$, $E_0=\pi^2\hbar^2/2m^*L^2$, ϕ_N represents the harmonic oscillator wave function centered at $x_0=-\lambda^2 k_y$ with $\lambda=(\hbar c/eB)^{1/2}$ being the cyclotron radius, and $\omega_c=(|e|B)/(m^*c)$ the cyclotron frequency with L being the thickness of the FSQW centered at $z=0$. The envelope function, $\chi_m(z)$, is

$$\chi_m(z) = \sqrt{\frac{2}{L}}\sin\left(\frac{m\pi z}{L} + \frac{m\pi}{2}\right). \quad (6)$$

C. Acoustic phonons in a free-standing quantum well layer

The elastic continuum model[2,24,25] provides the description of longitudinal acoustic phonons for nanostructures having a confined dimension of about few atomic monolayers. We consider a free-standing solid slab with unconstrained surfaces at $z=\pm L/2$. Neglecting the distortion of acoustic vibrations resulting from the contact with the semiconductor substrate, free-standing structures provide an extreme confinement limit for acoustic phonons. This leads to the quantization of the phonon wave vector in the z direction, i.e., the z component of confined mode wave vector, q_z, takes only discrete set of values for each in-plane wave vector $q_\perp$. The q_z quantization is based on the simple rule that an integral number of half wavelengths fit in a semiconductor slab of thickness L.

In the case of elastic isotropic medium, there are three different types of confined acoustic modes: shear waves, dilatational waves, and flexural waves. These modes are characterized by their distinctive spatial symmetries. In the following, expressions for various quantities are given in the Cartesian coordinate system with the x axis directed parallel to the vector $q_\perp$; $q_\perp=(q_x,0)$.

1. Shear waves

These waves have only one nonzero component, which is perpendicular to the direction of wave propagation and lies in the plane of quantum well.[2,24,25] The component of displacement is parallel to the surfaces $z=\pm L/2$, taking this nonzero taking component to be in the y direction, we have $u_n(q_\perp,z)=(0,u_y,0)$, with

$$u_y = \cos(q_{z,n}z) \text{ for } n = 0,2,4,\ldots,$$
$$\sin(q_{z,n}z) \text{ for } n = 1,3,5,\ldots, \quad (7)$$

and $q_{z,n}=n\pi/L$ with L being the thickness of the slab. These modes are similar to transverse modes in bulk semiconductor and are designated as rotational waves.[2] The dispersion relation for shear waves can be expressed as

$$\omega_n = s_t\sqrt{q_{z,n}^2 + q_x^2}, \quad (8)$$

where $s_t=\mu/\rho$ is the velocity of transverse acoustic waves in bulk semiconductors with μ being the Lame constant and ρ the density of semiconductor.

2. Dilatational waves

These modes are irrotational modes associated with compressional distortions of the medium.[2] The compressional character of these modes leads to local changes in the volume of the medium. These waves have two nonzero components,[2,24,25] $u_n(q_\perp,z)=(u_x,0,u_z)$, with

$$u_x = iq_x\left[(q_x^2 - q_t^2)\sin\frac{q_t L}{2}\cos q_l z + 2q_l q_t \sin\frac{q_l L}{2}\cos q_t z\right], \quad (9)$$

$$u_z = q_l\left[-(q_x^2 - q_t^2)\sin\frac{q_t L}{2}\sin q_l z + 2q_x^2 \sin\frac{q_l L}{2}\sin q_t z\right], \quad (10)$$

where q_l and q_t are solutions of

$$\frac{\tan(q_t L/2)}{\tan(q_l L/2)} = -\frac{4q_x^2 q_l q_t}{(q_x^2 - q_t^2)^2}, \quad (11)$$

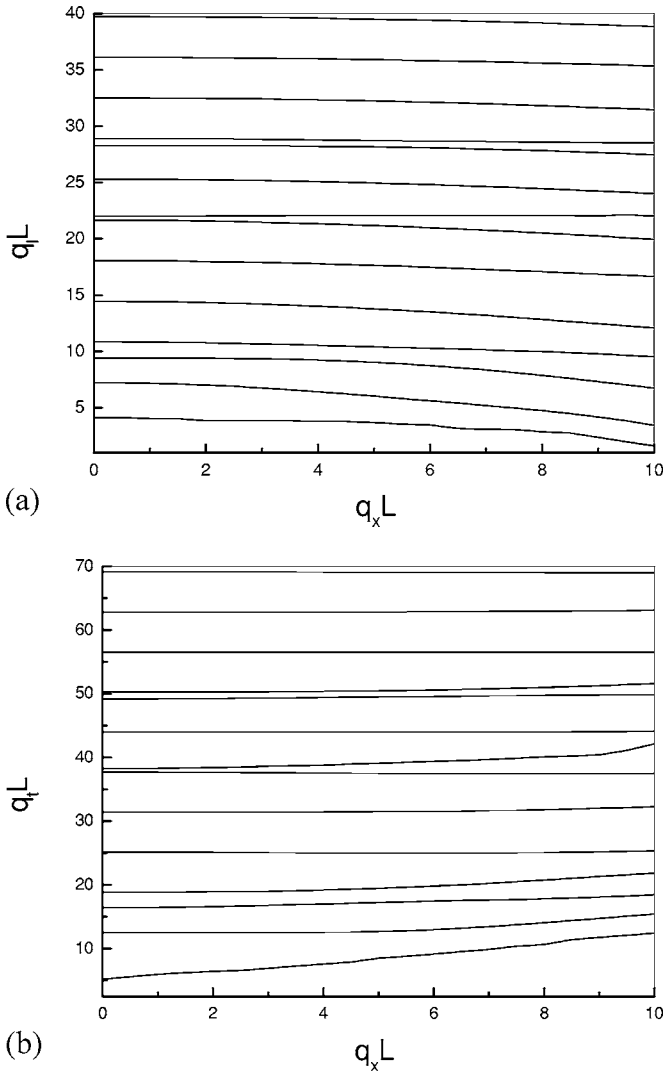

FIG. 1. The solutions (a) q_l and (b) q_t as a function of q_x for dilatational phonons in a GaN free standing quantum well.

$$s_l^2(q_x^2+q_l^2)=s_t^2(q_x^2+q_t^2). \tag{12}$$

The quantity s_l denotes the velocity of longitudinal acoustic waves in bulk semiconductors and is given by $s_l=(\zeta+2\mu)/\rho$ with ζ being the Lame constant. For each value of q_x, this pair of equations has either pure imaginary or real solutions,[27] denoted by $q_{l,n}(q_x)$ and $q_{t,n}(q_x)$. The label n is used to denote the different branches of the solutions $q_{l,n}(q_x)$ and $q_{t,n}(q_x)$. The dilatational waves have frequencies ω_n, satisfying

$$\omega_n=s_l\sqrt{q_x^2+q_{l,n}^2}=s_t\sqrt{q_x^2+q_{t,n}^2}. \tag{13}$$

Numerical solutions of Eqs. (11) and (12), in the case of GaN slab of thickness 10 nm for $s_l=8.77\times10^5$ cm/s and $s_t=5.041\times10^5$ cm/s, are shown in Figs. 1(a) and 1(b). The dispersion relation, for dilatational waves, calculated for a 10 nm thick GaN free-standing quantum well, is given in the Fig. 2.

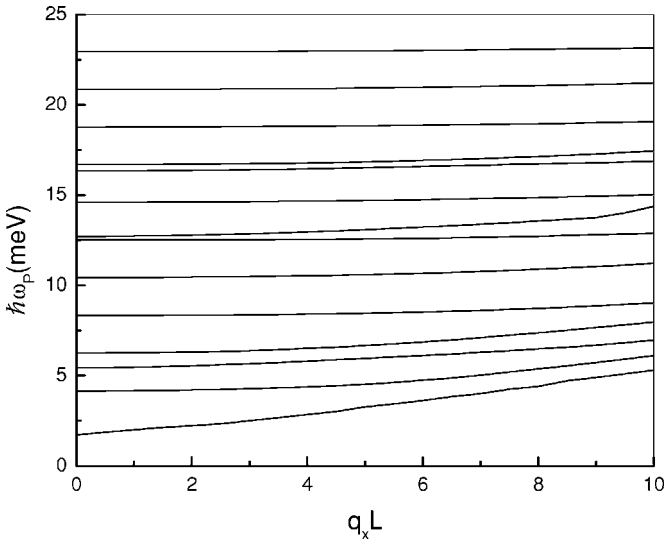

FIG. 2. Energy dispersion of the confined dilatational acoustic phonon modes in a GaN free-standing quantum well of thickness 10 nm.

3. Flexural waves

These are antisymmetric waves having two nonzero components,[2,24,25] $u_n(q_\perp,z)=(u_x,0,u_z)$, with

$$u_x=iq_x\left[(q_x^2-q_t^2)\cos\left(\frac{q_tL}{2}\right)\sin(q_lz)+2q_lq_t\cos\left(\frac{q_lL}{2}\right)\sin(q_tz)\right], \tag{14}$$

$$u_z=q_l\left[(q_x^2-q_t^2)\cos\left(\frac{q_tL}{2}\right)\cos(q_lz)-2q_x^2\cos\left(\frac{q_lL}{2}\right)\cos(q_tz)\right]. \tag{15}$$

q_l and q_t are now determined by solving the pair of equations,

$$\frac{\tan(q_lL/2)}{\tan(q_tL/2)}=-\frac{4q_x^2q_lq_t}{(q_x^2-q_t^2)^2}, \tag{16}$$

$$s_l^2(q_x^2+q_l^2)=s_t^2(q_x^2+q_t^2).$$

This pair of equations for flexural waves admits solutions of the form $q_{l,n}(q_x)$ and $q_{t,n}(q_x)$, where n labels the different branches of the solutions.[27] The frequencies and the solutions for $q_{l,n}$ and $q_{t,n}$ are different for dilatational and flexural modes.

D. Electron-phonon interaction

1. Electron-confined-acoustic-phonon interaction

Electrons in semiconductors are scattered by acoustic phonons through deformation potential interaction. The deformation potential depends on the strain tensor and deformation potential constant. For cubic crystals and for carriers experiencing a spherically symmetric energy surface, sym-

metry considerations make it evident that the crystalline potential is proportional to bulk strain. In the case of cubic crystal and for carriers at the nondegenerate Γ point, the Hamiltonian for electron-acoustic-phonon interaction is given by[2]

$$H_{el-ph} = E_d \nabla \cdot \mathbf{u},$$

where E_d is the deformation potential constant and $\mathbf{u}$ the displacement produced by a bulk acoustic mode of wave vector $\mathbf{Q}=(\mathbf{q}_\perp, q_z)$. In a FSQW, expression for electron-confined-acoustic-phonon interaction Hamiltonian can be written in the form[2,24,25]

$$H_{el-ph} = \sum_{q_\perp, n} \exp(i\mathbf{q}_\perp \cdot \mathbf{r})\Gamma_\alpha(\mathbf{q}_\perp, n, z)[a_n(\mathbf{q}_\perp) + a_n^\dagger(-\mathbf{q}_\perp)], \tag{17}$$

with

$$\Gamma_\alpha(\mathbf{q}_\perp, n, z) = F_{\alpha,n}\sqrt{\frac{\hbar E_d^2}{2A\rho\omega_n^\alpha(\mathbf{q}_\perp)}}(q_{t,n}^2 - q_x^2) \times (q_{l,n}^2 + q_x^2) tsc1_\alpha\left(\frac{Lq_{t,n}}{2}\right) tsc2_\alpha(q_{l,n}z), \tag{18}$$

where α distinguishes the dilatational (d) and flexural (f) confined-acoustic modes. The label $n=1,2,3\ldots$ is the index for different branches of confined modes, ρ the density of the material, and A the area of the FSQW structure. The symbols representing trigonometric functions are $tsc1_\alpha$=sin and $tsc2_\alpha$=cos if $\alpha=d$ (dilatational) and $tsc1_\alpha$=cos and $tsc2_\alpha$=sin if $\alpha=f$ (flexural). The function $F_{\alpha,n}$ is the normalization constant defined in terms of $q_{l,n}$ and $q_{t,n}$.[24] In the case of shear modes, $\Gamma_\alpha(\mathbf{q}_\perp, n, z)=0$. Hence shear waves do not interact with electrons through the deformation potential.

For the wave function given in Eq. (4), the matrix elements for electron-confined-acoustic-phonon interaction can be expressed as

$$\langle f|H_{el-ph}|i\rangle = C_{ph}(q_\perp, q_{t,n}, q_{l,n}) J_{NN'}(q_\perp) G_{mm'}^\alpha(q_{l,n}) \delta_{k_y', k_y+q_y}, \tag{19}$$

where

$$C_{ph} = F_{\alpha,n}\left(\frac{\hbar E_d^2}{2A\rho\omega_n^\alpha(q_\perp)}\right)^{1/2}(q_{t,n}^2 - q_x^2)(q_{l,n}^2 + q_x^2) tsc1_\alpha\left(\frac{Lq_{t,n}}{2}\right) \times \left(N_{q_\perp,n}^\alpha + \tfrac{1}{2} \mp \tfrac{1}{2}\right)^{1/2} \tag{20}$$

for $N' \geq N$, N_q is the Bose-Einstein distribution function given by

$$N_{q_\perp,n}^\alpha = \left[\exp\left(\frac{\hbar\omega_n^\alpha(q_\perp)}{k_B T}\right) - 1\right]^{-1}$$

and

$$\left|J_{NN'}\left(\frac{q_\perp \lambda}{2}\right)\right|^2 = \frac{n_2!}{n_1!} e^{-u} u^{n_1 - n_2}[L_{n_2}^{n_1-n_2}(u)]^2,$$

with $u=\lambda^2 q_\perp^2/2$, $n_1=\max(N,N')$, and $n_2=\min(N,N')$. $L_{n_2}^{n_1-n_2}$ are the associated Laguerre polynomials. The overlap integral function $G_{mm'}^\alpha$ is defined as

$$G_{mm'}^\alpha(q_z, q_{l,n}) = \int_{-L/2}^{L/2} \chi_{m'}^*(z) tsc2_\alpha(q_{l,n}z)\chi_m(z) dz.$$

2. Electron-bulk phonon interaction

Assuming acoustic-phonon modes in a FSQW are similar to those in a bulk semiconductor, the matrix elements for the electron-acoustic-phonon interaction through deformation potential can be expressed as

$$\langle f|H_{el-ph}|i\rangle = V(\mathbf{Q})\left(N_\mathbf{Q} + \tfrac{1}{2} \mp \tfrac{1}{2}\right)^{1/2} G_{mm'}(\pm q_z) \times J_{NN'}(\mathbf{q}_\perp)\delta_{k_y \pm q_y, k_y'}, \tag{21}$$

where N_Q is the Bose distribution function for phonons of wave vector $\boldsymbol{Q}$ and $V(\mathbf{Q})$ represents the strength of electron-acoustic-phonon interaction and is given by

$$|V(\mathbf{Q})|^2 = \frac{k_B T E_d^2}{2v^2\rho V}, \tag{22}$$

with v being the velocity of sound in the FSQW structure. The overlap integral, $G_{mm'}(q_z)$, is given by

$$G_{mm'}(\pm q_z) = \int_{-L/2}^{L/2} \chi_{m'}^*(z)\exp(\pm q_z z)\chi_m(z) dz. \tag{23}$$

E. Electron-photon interaction

The Hamiltonian for electron interaction with radiation field is given by[19]

$$H_{rad} = -\frac{e}{m^*}\left[\frac{2\pi N_\nu \hbar}{\Omega\varepsilon V}\right]^{1/2} \mathbf{e} \cdot \mathbf{P}, \tag{24}$$

where $\mathbf{e}$ is the polarization vector of radiation field, $\mathbf{P}=\mathbf{p}-(e/c)\mathbf{A}_0$ is the generalized momentum in static magnetic field, with Landau gauge vector potential $\mathbf{A}_0=(0, Bx, 0)$, N_ν is the number of photons in the radiation field, Ω the photon frequency, and ε the dielectric constant of the medium. Using the electron wave function in Eq. (4) and assuming the electromagnetic field to be linearly polarized transverse to the magnetic field, the matrix elements for photon absorption can be written as

$$\langle N+1|H_{rad}|N\rangle = \frac{e\hbar}{m^*}\left(\frac{2\pi N_\nu}{\hbar\Omega\varepsilon V}\right)^{1/2}\left(\frac{\hbar m^* \omega_c}{2}\right)^{1/2} \times (N+1)^{1/2}\delta_{N',N+1}\delta_{k_y k_y'}\delta_{mm'}. \tag{25}$$

F. Absorption coefficient

In the following we restrict ourselves to nondegenerate electron gas. In the presence of quantizing magnetic field, the

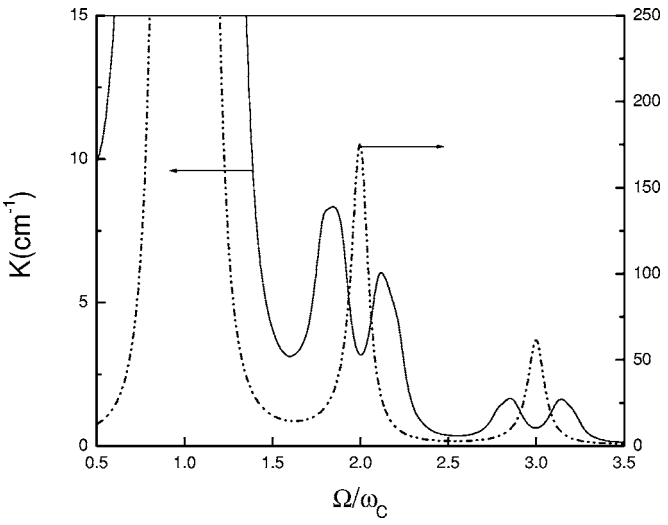

FIG. 3. Absorption spectrum due to confined (full curve) and bulk (dashed-dot-dot-curve) acoustic phonon modes is shown as a function of Ω/ω_C for GaAs slab of thickness 10 nm, at B=10 T and T=77 K.

distribution function, f_{Nm}, can be shown to be[19]

$$f_{Nm} = \frac{n_0 \pi \lambda^2 L}{\gamma} \exp\left(-\frac{E_{Nm}}{k_B T}\right), \tag{26}$$

where n_0 is the electron concentration and

$$\gamma = \sum_{N,m} \exp\left(-\frac{E_{Nm}}{k_B T}\right). \tag{27}$$

Using Eq. (1) and a straightforward calculation of transition probabilities and assuming the electromagnetic field to be linearly polarized transverse to the magnetic field, we obtain the following expression for PACR in a free-standing quantum well structure due to confined acoustic modes described by the elastic continuum model,

$$\begin{aligned} K_C(B) = {} & \frac{n_0 e^2 \omega_c E_d^2 \lambda^2}{8 m^* c \Omega \sqrt{\varepsilon} \rho \gamma} \left\{ \frac{1}{(\omega_c + \Omega)^2} + \frac{1}{(\omega_c - \Omega)^2} \right\} \\ & \times \sum_{m,N,m'N'} \exp\left(-\frac{E_{Nm}}{k_B T}\right) \sum_{\alpha,n} \int q_\perp^3 dq_\perp \frac{|F_{\alpha n}|^2}{\omega_n^\alpha(q_\perp)} \\ & \times (q_{t,n}^2 - q_x^2)^2 (q_{l,n}^2 + q_x^2)^2 tsc1_\alpha^2 \left(\frac{L q_{t,n}}{2}\right) \left| J_{NN'}\left(\frac{q_\perp \lambda}{2}\right) \right|^2 \\ & \times |G_{mm'}^\alpha(q_{l,n})|^2 \{ N_{q_\perp,n}^\alpha \delta[(m'^2 - m^2) E_0 \\ & + (N' - N)\hbar\omega_c - \hbar\omega_n^\alpha(q_\perp) - \hbar\Omega] \\ & + (N_{q_\perp,n}^\alpha + 1)\delta[(m'^2 - m^2) E_0 + (N' - N)\hbar\omega_c \\ & + \hbar\omega_n^\alpha(q_\perp) - \hbar\Omega] \}, \end{aligned} \tag{28}$$

where the subscript c refers to confined modes. In the extreme quantum limit ($m=m'=1$) the overlap integral $G_{mm'}^\alpha$ becomes

$$G_{11}^d(q_{l,n}) = \sin\left(\frac{q_{l,n} L}{2}\right) \left\{ \frac{2}{q_{l,n} L} + \frac{1}{(2\pi - q_{l,n} L)} - \frac{1}{(2\pi + q_{l,n} L)} \right\} \tag{29}$$

for dilatational modes and

$$G_{11}^f = 0 \tag{30}$$

for flexural modes. Thus, we see that only dilatational modes contribute to PACR in the extreme quantum limit.

The expression for absorption coefficient in the extreme quantum limit, for a FSQW,

$$\begin{aligned} K_c(B) = {} & \frac{n_0 e^2 \omega_c E_d^2 \lambda^2}{8 m^* c \Omega \sqrt{\varepsilon} \rho \gamma} \left\{ \frac{1}{(\omega_c + \Omega)^2} + \frac{1}{(\omega_c - \Omega)^2} \right\} \\ & \sum_{N,N'} \exp\left(-\frac{E_{N1}}{k_B T}\right) \sum_n \int q_\perp^3 dq_\perp \frac{|F_{dn}|^2}{\omega_n^d(q_\perp)} (q_{t,n}^2 - q_x^2)^2 \\ & (q_{l,n}^2 + q_x^2)^2 tsc1_d^2 \left(\frac{L q_{t,n}}{2}\right) \\ & \times \left| J_{NN'}\left(\frac{q_\perp \lambda}{2}\right) \right|^2 |G_{11}^d(q_{l,n})|^2 \{ N_{q_\perp,n}^d \delta[(N' - N)\hbar\omega_c \\ & - \hbar\omega_n^d(q_\perp) - \hbar\Omega] + (N_{q_\perp,n}^d + 1)\delta[(N' - N)\hbar\omega_c \\ & + \hbar\omega_n^d(q_\perp) - \hbar\Omega] \} \end{aligned} \tag{31}$$

Using the matrix element for electron-bulk acoustic-phonon interaction [Eq. (21)] we have also obtained following expression for PACR, in extreme quantum limit, in a FSQW:

$$\begin{aligned} K_b(B) = {} & \frac{3\pi n_0 e^2 \omega_c E_d^2 k_B T}{16 m^* c \Omega \sqrt{\varepsilon} \rho v^2 \gamma \hbar \lambda^2 L} \left\{ \frac{1}{(\omega_c + \Omega)^2} + \frac{1}{(\omega_c - \Omega)^2} \right\} \\ & \times \sum_{N,N'} \exp\left(-\frac{E_{Nm}}{k_B T}\right) (N' + N + 1)\delta[(N' - N)\hbar\omega_c \\ & - \hbar\Omega], \end{aligned} \tag{32}$$

where the subscript b refers to bulk description of acoustic modes. This can be compared with the expression [Eq. (31)] obtained with confined description of acoustic modes.

III. RESULTS AND DISCUSSION

We have evaluated numerically the expression for PACR absorption coefficient [Eq. (31)] for GaAs and GaN FSQWs. The material parameters used, in the case of GaAs, are[24,28,30] $m^*=0.067m_0$, $E_d=12.42$ eV, $\varepsilon=11.56$, $\rho=5.31$ g/cm^3, $v=5.22\times10^5$ cm/s, $s_l=5.7\times10^5$ cm/s, $s_t=3.35\times10^5$ cm/s, and $n_o=1\times10^{17}$ cm^{-3}. The Dirac delta functions in Eq. (31) are replaced by Lorentzian of width Γ. A value of 1 meV is used for the width Γ. This value has been chosen on the basis of self-consistent calculations of the electron scattering rate due to confined-acoustic modes in the presence of a magnetic field. Figure 3 shows the variation of absorption coefficient, K_c, with Ω/ω_C (full curve), in the case of GaAs FSQW of thickness $L=10$ nm, at $T=77$ K and $\mathbf{B}=10$ T. For comparison, we have evaluated numerically the absorption coeffi-

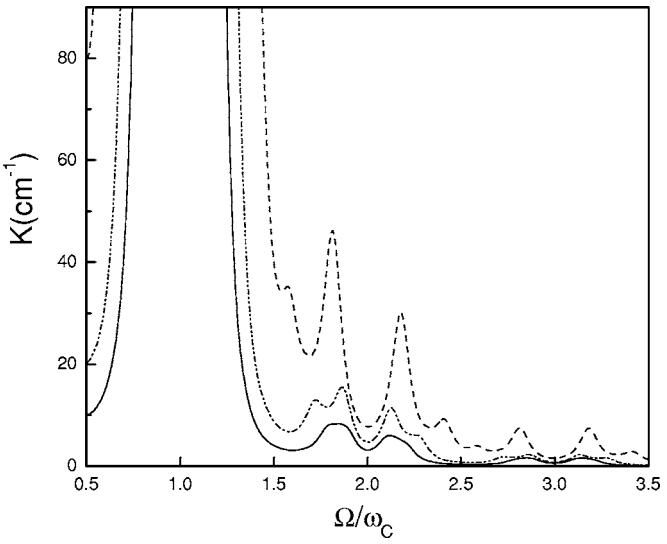

FIG. 4. Quantum slab thickness dependence of absorption coefficient due confined modes in GaAs slab at B = 10 T and T = 77 K. The dashed curve is for 5 nm, dashed-dot-dot curve for 7.5 nm and the full curve for 10 nm thickness.

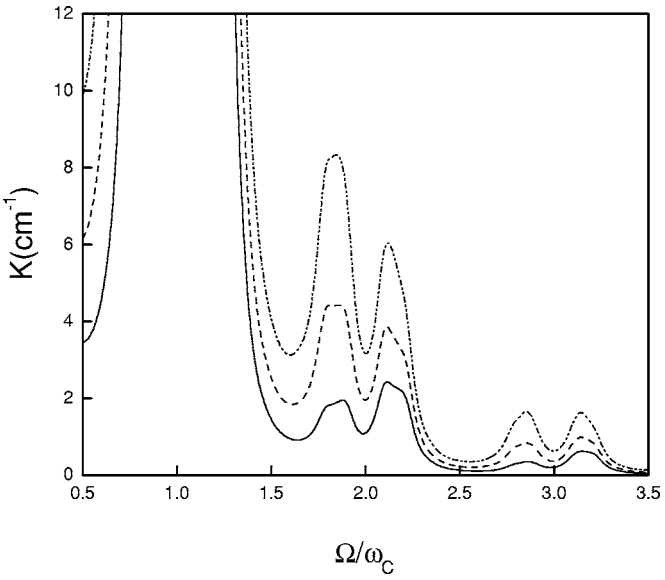

FIG. 5. Temperature dependence of PACR absorption coefficient, K, due to confined modes in GaAs slab of thickness 10 nm at B = 10 T. The full curve is for 27 K, dashed curve for 50 K and dashed-dot-dot curve for 77 K.

cient [Eq. (32)] obtained with the bulk description of phonon modes (shown as the dashed-dot-dot curve). The singularity at $\Omega=\omega_C$ is due to the term $(\Omega-\omega_C)^{-2}$ in the expression for PACR [see Eqs. (31) and (32)]. The additional peaks in case of confined modes (full curve) are due to PACR, whereas in the bulk description of phonon modes (dashed-dot-dot curve) the peaks are due to pure cyclotron resonance. The PACR transitions are of different types[19] depending upon the Landau-level separation, photon, and phonon energies. The conditions for resonant transitions can be written as $\Omega=\eta\omega_C\pm\omega_n^d(q_\perp)$ with $\eta=1,2,3\ldots$ and $\omega_n^d(q_\perp)$ being the frequency of nth dilatational acoustic mode. Although energy of each mode is different, its variation with wave vector is small. Therefore, the frequency of phonon mode is denoted as ω_p. In the case of pure cyclotron resonance, the electron transition between Landau levels occurs with the absorption of a photon with frequencies $\Omega=\eta\omega_C$, whereas in PACR the resonant transfer of electrons between Landau levels is due to involvement of both photon and a phonon. The peak at $\Omega/\omega_C=1.846$ is due to absorption of confined-acoustic phonon with energy 2.66 meV and the one at $\Omega/\omega_C=2.11$ is due to emission of a phonon with energy 2.05 meV. Both these peaks correspond to the transition with $\eta=2$. The peak at $\Omega/\omega_C=2.86$ is due to acoustic phonon with energy 2.57 meV and that at $\Omega/\omega_C=3.141$ is due to the phonon with energy 2.48 meV. These transitions correspond to $\eta=3$. In all these transitions, the energy of the phonon mode is smaller than the Landau-level separation and transitions correspond to the type 1 in Ref. 19, which represents resonance transfer of electrons with absorption of photon followed by absorption/emission of phonons. Although there exist modes with higher energy, their contribution to PACR is negligibly small. The maximum contribution is from the $n=1$ mode followed by $n=2$ and 3, but peaks due to the latter are not distinctly visible as their peak positions nearly coincide with that of mode 1 and also peak values are smaller than that due to the first mode.

Figure 4 shows the FSQW slab thickness dependence of absorption coefficient calculated for GaAs slabs for **B** = 10 T and $T=77$ K. The dashed curve is for 5 nm, the dashed-dot-dot curve for 7.5 nm, and the full curve is for 10 nm thick FSQW structures. It may be noted that with the decrease in thickness of the slab, the peak value of absorption coefficient increases and also the peaks become sharper. The energy of a confined mode decreases with increasing thickness of the slab. At lower thickness of the slab, contribution from high-energy mode decreases and peaks become sharp. As the energy of the mode decreases at higher thickness, many modes participate and peaks become broad.

Figure 5 shows the temperature dependence of K_c with Ω/ω_C for a GaAs slab of thickness 10 nm and for **B** = 10 T. The full curve is for $T=27$ K, dashed curve for 50 K, and dashed-dot-dot curve for 77 K. We observe that the peak value of absorption coefficient increases with increasing temperature. As the temperature increases, contribution due to all the modes increases, leading to a general increase in the magnitude of absorption coefficient. At lower temperatures, the absorption due to many of the lower energy modes becomes comparable and peaks become broad. As the optical modes begin to contribute at temperatures greater than 50 K, the contributions of confined acoustic modes can be detected from studies at lower temperatures ($T<50$ K).

In Fig. 6 we have shown the variation of K_c with applied magnetic field as a function of Ω/ω_C for a GaAs slab of thickness 10 nm at $T=77$ K. The dotted curve is for **B** = 5 T, dashed-dot-dot curve for 10 T, and the full curve for 15 T. The peak values of K_c become sharper at higher magnetic field. As Landau-level separation increases, only few phonon modes contribute to PACR. At higher magnetic field, modes with energy comparable to cyclotron energy contribute and other modes become negligible for the range of temperatures studied. The peaks in the full curve at Ω/ω_C

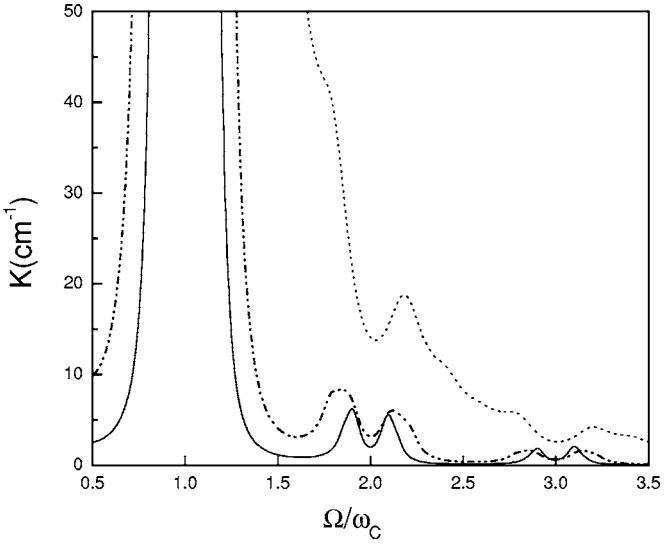

FIG. 6. Magnetic field dependence of PACR absorption coefficient due to confined modes is shown for GaAs slab of thickness 10 nm at T=77 K. The dotted curve is for 5 T, dashed-dot-dot curve for 10 T and the full curve for 15 T.

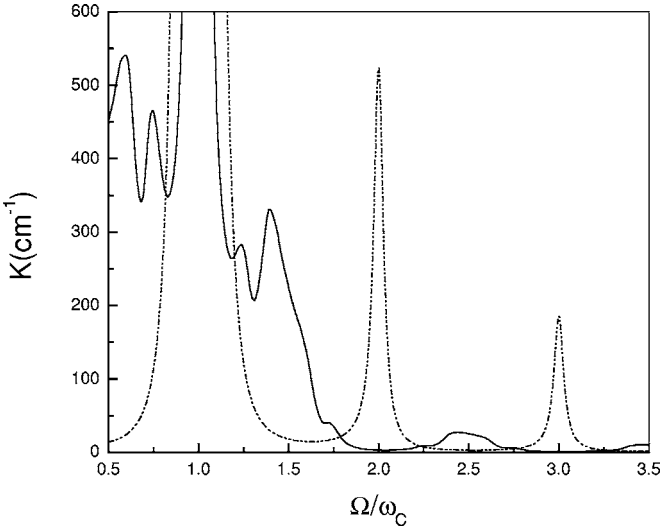

FIG. 7. Absorption spectrum in case of GaN free standing quantum well slab is shown as a function of Ω/ω_C of thickness of 10 nm at B=10 T and T=77 K. Full curve is for confined acoustic phonon modes and dashed-dot-dot curve is for bulk description of phonon modes.

=1.90 and 2.096 are due to 2.598 meV and 2.494 meV modes, respectively. At lower magnetic fields, the contribution due to lower energy modes increases and kinks in the dotted curve indicate the participation of multiple modes. The peak positions in the absorption spectrum at higher field can therefore be used to estimate the energy of the confined modes involved in PACR.

We have also evaluated Eq. (31) and Eq. (32) in the case of GaN FSQW structure. The material parameters characteristic of GaN with zinc-blende structure are,[29,30] $m^*=0.15m_0$, $E_d=10$ eV, $\varepsilon=9.5$, $\rho=6.1$ g/cm^3, and $v=4.57\times10^5$ cm/s. Figure 7 shows the variation of K_c with Ω/ω_C for a GaN slab of thickness $L=10$ nm, at $\mathbf{B}=10$ T and $T=77$ K. For width parameter Γ, a value of 0.25 meV is used based on self-consistent calculation of the electron scattering rate in GaN. The full curve is for confined-acoustic modes and the dotted curve is for bulk description of acoustic modes. The general features of absorption spectrum are the same as those seen in the case of GaAs, except the peak positions and sharpness of peaks. The peak value at $\Omega/\omega_C=0.596$ is due to the first mode with energy 3.136 meV, and the one at $\Omega/\omega_C=0.746$ is due the third mode with energy 5.73 meV. These transitions are of type III given in Ref. 19, which correspond to PACR transitions when ω_c is smaller than ω_p and $\Omega<\omega_p$. The peak at $\Omega/\omega_C=1.236$ is due to transition corresponding to $\eta=2$ and involving phonon mode with $\eta=3$ and energy 5.89 meV. The transition is of type I in Ref. 19. The peak at $\Omega/\omega_C=1.396$ corresponds to the emission of a phonon with energy 3.05 meV. The peak at $\Omega/\omega_C=1.721$ corresponds to $\eta=1$ and involves emission of third phonon mode with energy 5.56 meV. Similarly, the peak at $\Omega/\omega_C=2.436$ is due to absorption of first-mode phonon with energy 3.36 meV and with $\eta=2$. In all these transitions, the energy of the phonon mode is smaller than the Landau-level separation, which is 7.715 meV at a magnetic field of 10 T. The absorption spectrum, therefore, has peaks on either sides of $\Omega/\omega_C=1$. The maximum contribution is from the first mode followed by the second and the third modes. The peaks due the modes with higher energy are not visible. The bulk description of phonon modes gives only the pure cyclotron resonance absorption spectrum. The energy of the photon involved in the resonant transfer of electron is lower than that in GaAs.

Figure 8 shows the variation of absorption coefficient with temperature. The full curve is for T=27 K, dashed-dot-dot curve for 50 K, and the dotted curve is for 77 K. The absorption coefficient increases with increasing temperature and peaks, in general, become clear at higher temperatures. In Fig. 9 we have shown the magnetic field dependence of

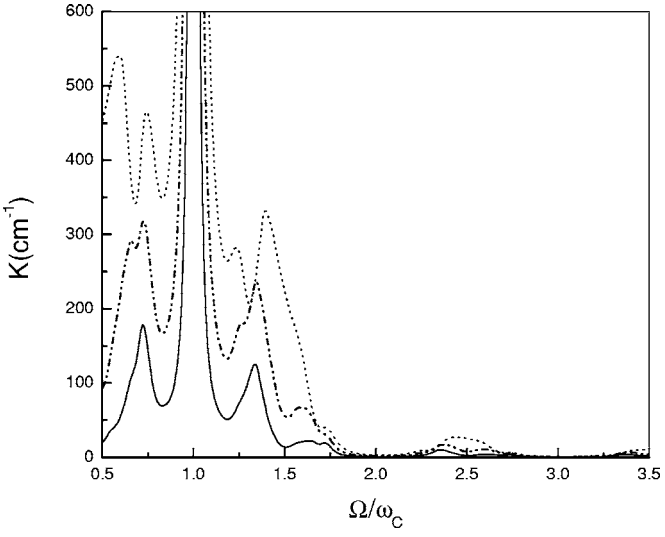

FIG. 8. Temperature dependence of absorption coefficient due to confined mode in GaN slab 10 nm at B=10 T. The full curve is for 27 K, dashed-dot-dot curve for 50 K and the dotted curve is for 77 K.

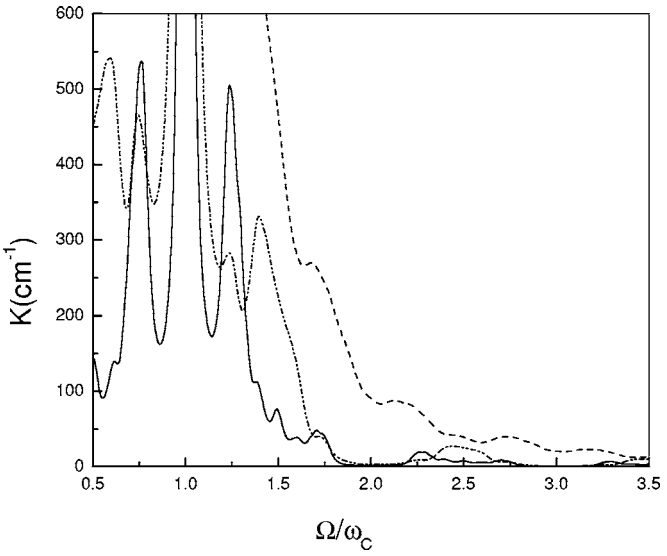

FIG. 9. Magnetic field dependence of absorption coefficient due to confined modes in a GaN slab of thickness 10 nm at T=77 K. The dashed curve is for 5 T, dashed-dot-dot curve 10 T and the full curve is for 15 T.

the absorption coefficient in the case of a GaN slab of thickness 10 nm at $T=77$ K. The dashed curve is for 5 T, the dashed-dot-dot curve for 10 T, and the full curve is for 15 T. The sharpness of the peaks increases with the increasing magnetic field. The peaks, in full curve, both at $\Omega/\omega_C=0.761$ and $\Omega/\omega_C=1.236$, involve the phonon of energy 2.765 meV corresponding to first mode. For $\mathbf{B}=5$ T the absorption peak at $\Omega/\omega_C=1.676$ is also due to first confined mode and the transition is of type I as given in Ref. 19. At higher fields, modes with energy comparable to Landau-level separation contribute to PACR. The peaks in full curve ($\mathbf{B}=15$ T) are due to involvement of high-energy modes.

From the above results we see that the absorption spectrums of GaAs and GaN have similar features and the presence of various confined modes in FSQW can easily be detected in a PACR experiment. From studying the peak positions, one can determine the characteristic energies of phonon modes involved in the PACR.

IV. CONCLUSIONS

We have studied phonon-assisted cyclotron resonance, due to electron interaction with confined-acoustic-phonon modes, in free-standing quantum well structures. Numerical results are presented for GaAs and GaN systems by including the dispersive nature of confined modes. In the extreme quantum limit, flexural modes do not contribute. Results are presented for the frequency, magnetic field, temperature, and well-width dependence of absorption coefficient. Broadly, the features are similar in both the systems. The absorption spectrum consists of additional peaks due to electron-confined-acoustic-mode interaction compared to the spectrum with bulk description of phonons. It is noticed that only few low-energy confined modes contribute significantly to PACR. The peak value of the absorption coefficient is found to increase with increasing temperature and magnetic field but to decrease with increasing thickness of the slab. In contrast to GaAs, in the case of GaN system, the peaks are broader. In general, sharpness of the peaks increases with increasing temperature and magnetic field. As only few confined modes contribute to PACR, significant differences are noticeable in the magnitude of the absorption spectrum as compared with results obtained with bulk description of phonons. It is concluded that PACR studies lead to a better understanding of confined electron-phonon interaction in FSQW structures.

ACKNOWLEDGMENT

This work was supported by UGC-India.

*Corresponding author.

[1] V. V. Mitin, V. A. Kochelap, and M. A. Stroscio, *Quantum Heterostructures* (Cambridge University Press, Cambridge, England, 1999).
[2] M. A. Stroscio and Mitra Dutta, *Phonons in Nanostructures* (Cambridge University Press, Cambridge, England, 2001).
[3] F. G. Bass and I. B. Levinson, Zh. Eksp. Teor. Fiz. **49**, 914 (1965) [Sov. Phys. JETP **22**, 635 (1966)].
[4] R. K. Bakanas, Fiz. Tverd. Tela (Leningrad) **12**, 3408 (1971) [Sov. Phys. Solid State **12**, 2769 (1971)].
[5] T. M. Rynne and H. N. Spector, J. Appl. Phys. **52**, 393 (1981).
[6] M. W. Goodwin and D. G. Seiler, Phys. Rev. B **27**, 3451 (1983).
[7] R. C. Enck, A. S. Saleh, and H. Y. Fan, Phys. Rev. **182**, 790 (1969).
[8] E. J. Johnson and D. H. Dickey, Phys. Rev. B **1**, 2676 (1970).
[9] M. Singh and B. Tanatar, Phys. Rev. B **41**, 12781 (1990).
[10] B. Tanatar and M. Singh, Phys. Rev. B **42**, 3077 (1990).
[11] J. S. Bhat, S. S. Kubakaddi, and B. G. Mulimani, J. Appl. Phys. **70**, 2216 (1991).
[12] M. V. Klein, IEEE J. Quantum Electron. **QE-22**, 1760 (1986).
[13] B. Jessurand and M. Cardona, in *Light Scattering in Solids V*, edited by M. Cardona and G. Guntherodt (Springer, Heidelberg 1989).
[14] L. Wendler and R. Pechstedt, Phys. Status Solidi B **141**, 129 (1987).
[15] L. Wendler, Phys. Status Solidi B **129**, 513 (1985).
[16] L. Wendler and V. G. Grigoryan, Surf. Sci. **206**, 203 (1988).
[17] L. Wendler, V. M. Fomin, A. V. Chaplik, and A. O. Govorov, Phys. Rev. B **54**, 4794 (1996).
[18] G. Q. Hai, F. M. Peeters, and J. T. Devreese, Phys. Rev. B **47**, 10358 (1993).
[19] J. S. Bhat, B. G. Mulimani, and S. S. Kubakaddi, Phys. Rev. B **49**, 16459 (1994).
[20] M. Grimsditch, R. Bhadra, and I. K. Schuller, Phys. Rev. Lett. **58**, 1216 (1987).
[21] R. Bhadra, M. Grimsditch, I. K. Schuller, and F. Nizzoli, Phys.

Rev. B **39**, 12456 (1989).
[22] M. D. Williams, S. C. Shunk, M. G. Young, D. P. Doctor, D. M. Tennant, and B. I. Millar, Appl. Phys. Lett. **61**, 1353 (1992).
[23] A. Balandin and K. L. Wang, Phys. Rev. B **58**, 1544 (1998).
[24] N. Bannov, V. Aristov, V. V. Mitin, and M. A. Stroscio, Phys. Rev. B **51**, 9930 (1995); Phys. Status Solidi B **183**, 131 (1994).
[25] N. A. Bannov, V. V. Mitin, and M. Stroscio, *Quantum Transport in Ultrasmall Devices* (Plenum, New York, 1995).
[26] H. Meyer, Phys. Rev. **112**, 298 (1958).
[27] Physical Acoustics, Vol. 1, Part A, edited by W. Mason (Academic Press, New York, 1964).
[28] S. Adachi, J. Appl. Phys. **58**, R1 (1985).
[29] V. Gruzinskis, P. Shiktorov, and Jian H. Zhao, Supercond. Sci. Technol. **16**, 798 (2001).
[30] I. Vurgaftman, J. R. Meyer, and L. R. Ram-Mohan, J. Appl. Phys. **89**, 5815 (2001).